

## Differential-Operator and Correlated-Sampling Methods with Electron-Photon Transport in the Integrated TIGER Series

Brian C. Franke, Aaron Olson, Shawn D. Pautz

Sandia National Laboratories, P.O. Box 5800, Albuquerque, NM  
bcfrank@sandia.gov, aolson@sandia.gov, sdpautz@sandia.gov

**Abstract** - Several techniques have been developed in the radiation transport community for the calculation of sensitivities in Monte Carlo simulations. We have been investigating application of these techniques to coupled electron-photon transport building on recently developed single-scattering electron-transport algorithms in the Integrated TIGER Series (ITS) codes. Our efforts have focused specifically on the differential-operator and correlated-sampling methods. In a simplified problem, we verify the accuracy of the two methods used in conjunction by comparison with semi-analytic results. We present sensitivity results from the differential-operator method for two test problems based on validation experiments. We verify the accuracy of the sensitivities by comparison with approximate values calculated by the central-differencing approach. We have found that the correlated-sampling method is generally unstable for electron transport, which we attribute to the large interaction cross sections and lack of particle absorption.

### I. INTRODUCTION

Sensitivity-estimation techniques in Monte Carlo radiation transport have existed for more than 30 years [1] and are valuable for uncertainty quantification, but they have not previously been extended to electron transport. Building on a recently implemented single-scatter electron transport algorithm, we are developing methods for calculating both sensitivities to cross sections and finite perturbations in cross sections to enable computationally efficient uncertainty quantification.

There are multiple uncertainty-quantification techniques that can utilize gradients (i.e., sensitivities), and various methods and references are given in the Dakota user manual [2]. Reliability methods use gradient-based optimization solvers. Gradient-enhanced polynomial chaos expansions (PCE) use both function values and gradients to build a surrogate model. These approaches are applied to a satellite-shielding application with sensitivities from deterministic transport in Ref. [3].

The differential-operator method has been extensively investigated for calculation of sensitivities in neutron and photon transport [4, 5, 6]. Correlated sampling is an approach less suitable for calculating sensitivities than for finite perturbations [4, 5]. Using this method to evaluate a transport problem at multiple finite perturbations has previously been investigated for constructing PCE models [7, 8].

To implement these methods, we are using a new electron transport implementation in ITS based on the LLNL evaluated data libraries [9, 10, 11]. This approach avoids the difficulties of adapting the methods to a condensed history algorithm. One possible challenge in applying both methods to electron transport is the large number of interactions that electrons undergo. Theoretical limitations of the methods were previously explored by Rief [4]. Here we offer demonstrations of the methods for simple problems, but the practical and theoretical limitations of the methods as applied to electron transport remain to be explored in future work.

In Section II, we present the correlated-sampling and differential-operator methods. In Section III, we describe a semi-analytic benchmark and use it to test the combined meth-

ods for a simple monoenergetic problem. In Section IV, we show sensitivities calculated using the differential-operator method for electron-photon transport problems and demonstrate the correctness of the results by comparison with central-difference perturbations.

### II. THEORY

In our Monte Carlo implementation we are interested in applying both a correlated sampling method for evaluating results of perturbed problems and a differential operator method for evaluating sensitivities. The correlated-sampling method uses multiplicative particle-weight adjustments, like Monte Carlo biasing methods. The differential-operator method accumulates sensitivity weights through additive adjustments. The particle weights affected by correlated sampling are used in all tallies. The sensitivity weights affected by the differential operator are used only in sensitivity tallies. The two types of weights are accumulated independently and are multiplied when tallying sensitivity for a response. In the following sections we discuss in more detail how the weights are used in tallies and adjusted during the Monte Carlo simulation.

Because both the correlated-sampling and differential-operator techniques do not change the random number sequence of the nominal problem, one can evaluate as many correlated-sampling states and associated differential-operator sensitivities as desired in a single Monte Carlo simulation. However, it does require that the code accumulate the associated weights for each problem state. Every tally (for which such results are desired) must also accumulate results for each problem state and sensitivity.

Monte Carlo radiation transport can be described as solving a Fredholm-type integral equation of the second kind [5, 12]:

$$\chi(\mathbf{x}) = \int_R K(\mathbf{x} \leftarrow \mathbf{y})\chi(\mathbf{y})dR + Q(\mathbf{x}), \quad (1)$$

where  $\chi$  is the collision density,  $K$  is the transport/collision transition kernel,  $R$  is the integration space, and  $Q$  is the source.

The Monte Carlo random-walk process can be interpreted as solving this integral equation by evaluating the terms of a Neumann series:

$$\chi(\mathbf{x}) = \sum_{n=0}^{\infty} \chi_n(\mathbf{x}), \quad (2)$$

$$\chi_0(\mathbf{x}) = Q(\mathbf{x}), \quad (3)$$

$$\chi_n(\mathbf{x}) = \int_R K(\mathbf{x} \leftarrow \mathbf{y}) \chi_{n-1}(\mathbf{y}) dR, n > 0. \quad (4)$$

In abbreviated notation, this process is

$$\begin{aligned} \chi(\mathbf{x}) &= \sum_{n=0}^{\infty} \int_R \cdots \int_R \left( \prod_{j=0}^n dy_j K(\mathbf{y}_{j+1} \leftarrow \mathbf{y}_j) \right) Q(\mathbf{y}_0) \\ &\equiv \sum_{n=0}^{\infty} \int_R \cdots \int_R \left( \prod_{j=0}^n dy_j K_j \right) Q(\mathbf{y}_0), \end{aligned} \quad (5)$$

where  $\mathbf{y}_{n+1} = \mathbf{x}$ . In an analog simulation, particle weights are unity, but in a biased simulation particle weights will vary. In correlated sampling, the process can remain the same, but weight adjustments are used to evaluate an alternative problem with a different solution. In this process we can separate particle-weight adjustments from the associated process as

$$\hat{\chi}(\mathbf{x}) = \sum_{n=0}^{\infty} \int_R \cdots \int_R \left( \prod_{j=0}^n w_j \right) \left( \prod_{j=0}^n dy_j K_j \right) Q(\mathbf{y}_0), \quad (6)$$

where the  $w_j$  are multiplicative weight adjustments. For correlated sampling these are determined by a likelihood ratio,  $\hat{K}_j/K_j$ .

Similarly, the sensitivity of the solution can be expressed as

$$p_i \frac{\partial \chi(\mathbf{x})}{\partial p_i} = \sum_{n=0}^{\infty} \int_R \cdots \int_R \left( \sum_{j=0}^n \beta_{i,j} \right) \left( \prod_{j=0}^n dy_j K_j \right) Q(\mathbf{y}_0), \quad (7)$$

where the sensitivity weights are

$$\beta_{i,j} = \frac{p_i}{K_j} \frac{\partial K_j}{\partial p_i}, \quad (8)$$

and the partial derivatives of  $K_j$  with respect to simulation parameters  $p_i$  are defined by the differential-operator method.

In practice, the accumulated product of sensitivity weights is maintained during the simulation:

$$W_n = \prod_{j=0}^n w_j. \quad (9)$$

Likewise, a running summation of sensitivity weights is maintained:

$$\gamma_{i,n} = \sum_{j=0}^n \beta_{i,j}. \quad (10)$$

A sensitivity,  $S_i$ , can be estimated in a process with biasing or correlated-sampling weight adjustments as

$$\begin{aligned} S_i &\equiv \frac{p_i}{\hat{\chi}(\mathbf{x})} \frac{\partial \hat{\chi}(\mathbf{x})}{\partial p_i} \\ &= \frac{1}{\hat{\chi}(\mathbf{x})} \sum_{n=0}^{\infty} \int_R \cdots \int_R W_n \gamma_{i,n} \left( \prod_{j=0}^n dy_j K_j \right) Q(\mathbf{y}_0). \end{aligned} \quad (11)$$

## 1. Correlated-Sampling Method

The correlated-sampling method is described in detail by Lux and Koblinger [5] and Rief [12]. Rief examined the stability limits of the method for infinite medium problems [4]. We have previously implemented the method for use with the stochastic-collocation method and examined stability limitations in our implementation [7]. The method is especially limited for problems with scattering ratios near unity and insufficient leakage. Electrons have very large scattering cross sections and no absorption cross section per se. However, electrons have a finite range in material, and in practice are only tracked until they fall below a cutoff energy. For some select problems, the cutoff energy may provide sufficient removal of particles from the problem.

Particles begin with a particle weight of unity (unless source biasing is used). Particle weights may also be adjusted during the simulation due to any biasing games applied to the simulation, but here we discuss only the weight adjustments for cross-section perturbations. As particles are tracked according to the cross sections of a nominal problem, the particle-weight adjustments are made according to a likelihood ratio

$$w_j = \frac{p_{pert,j}}{p_{sim,j}}. \quad (12)$$

That is, the particle-weight adjustment multiplier  $w_j$  of the particle at the end of segment  $j$  is the weight at the end of the previous segment times the ratio of the probability  $p_{pert,j}$  of the track occurring in the alternative ‘‘perturbed’’ state of the problem to the probability  $p_{sim,j}$  of the track as it was actually simulated in the nominal state of the problem. For accuracy each event outcome in the perturbed state must be possible in the nominal state, and for stability and good convergence behavior the probability ratio must not be too large.

Perturbations in an interaction cross section, density, or material composition can be accounted for by particle-weight adjustments during interactions and during particle streaming, either to a collision or to a boundary. The particle-weight adjustment after the particle interaction is

$$w_j = \frac{\Sigma_i^*(E')/\Sigma_t^*(E')}{\Sigma_i(E')/\Sigma_t(E')}, \quad (13)$$

where  $\Sigma_i$  divided by  $\Sigma_t$  is the probability of sampling interaction type  $i$  in the nominal problem, and the asterisk denotes the perturbed problem. The particle-weight adjustment in streaming to an interaction is

$$w_j = \frac{\Sigma_i^*(E) \exp(-\Sigma_t^*(E)\lambda_j)}{\Sigma_i(E) \exp(-\Sigma_t(E)\lambda_j)}, \quad (14)$$

where  $\Sigma_i^*$  is the perturbed interaction cross section,  $\Sigma_t$  is the simulated interaction cross section, and  $\lambda_j$  is the streaming distance. The particle-weight adjustment in streaming to a boundary is

$$w_j = \frac{\exp(-\Sigma_t^*(E)\lambda)}{\exp(-\Sigma_t(E)\lambda)}. \quad (15)$$

## 2. Differential-Operator Method

The differential-operator method is described by Lux and Koblinger [5] and Rief [12], and a derivation is given by Hess [6], of which we only note a few key points. To calculate the sensitivities we need the sensitivity weights (i.e., the partial derivatives,  $\beta_{i,j}$ ) defined in Eq. 8. These are given by

$$\beta_{i,j} = \delta_{i,a} - \frac{\Sigma_i(E')}{\Sigma_t(E')} - \Sigma_i(E)\lambda_j + \frac{\Sigma_i(E)}{\Sigma_t(E)}, \quad (16)$$

where  $\Sigma_t$  is the total macroscopic cross section, “ $a$ ” is a sampled interaction type, and  $\lambda_j$  is a sampled particle streaming distance.

Particles begin with a sensitivity weight of zero. Sensitivity-weight accumulations may be either positive or negative, and they are additive rather than multiplicative. After any collision tallies, the contribution is incremented by unity only for sensitivity to the sampled interaction, then contributions are accumulated as  $-\Sigma_i(E')/\Sigma_t(E')$ . For each particle streaming event, whether to an interaction or a boundary, contributions due to sensitivity to cross sections  $\Sigma_i$ , whether total or specific interaction cross sections, are each accumulated as  $-\Sigma_i\lambda_j$ . For sensitivity to a specific interaction cross section, the contributions are accumulated at the collision as  $\Sigma_i(E)/\Sigma_t(E)$ .

This explanation is simplified but consistent with our implementation, in which, for example, we are examining sensitivity to each cross section across all energies. The references provide details that arise in accounting for sensitivities as a function of energy, sensitivities in the tally response, and other complications.

## III. SEMI-ANALYTIC BENCHMARK COMPARISON

To test the approach of combining the correlated-sampling and differential-operator methods, we use a simple monoenergetic problem with isotropic scattering. The source is normally incident ( $\mu_0 = 1$ ) on a semi-infinite slab, and we compare the angle-integrated flux at the incident boundary.

The angular flux exiting the slab boundary is expressed [13]:

$$\psi(0, -\mu) = \frac{c}{2} \frac{\mu_0}{\mu + \mu_0} H(\mu_0)H(\mu), \quad (17)$$

where  $H$  is Chandrasekhar’s  $H$ -function and  $c$  is the scattering ratio,  $\frac{\sigma_s}{\sigma_t}$ . The  $H$ -function can be evaluated approximately as [14]

$$H(\mu) = 1 + \mu \sum_{i=1}^N \frac{a_i}{1 + s_i\mu} \quad (18)$$

in terms of  $s_i$  and  $a_i$ , which are solved using  $N$ -order Gauss-Legendre quadrature with nodes and weights  $\mu_i$  and  $w_i$ :

$$1 - c \sum_{i=1}^N \frac{w_i}{1 - \mu_i^2 s^2}; \quad \sum_{i=1}^N \frac{a_i}{1 - s_i\mu_k} = \mu_k^{-1}, \quad k = 1, \dots, N. \quad (19)$$

The derivative of the  $H$ -function is given in Ref. [15] as

$$\frac{dH(\mu)}{d\mu} = \frac{\mu H(\mu)}{c} \sum_{i=1}^N \frac{a_i H(s_i^{-1})}{1 + s_i\mu}. \quad (20)$$

The derivative of the angular flux with respect to the scattering ratio is therefore:

$$\frac{d\psi(0, -\mu)}{dc} = \frac{\mu_0}{2(\mu + \mu_0)} \left[ \left( \frac{dc}{d\mu_0} H(\mu_0)H(\mu) \right) + c \left( \frac{dH(\mu_0)}{d\mu_0} H(\mu) + H(\mu_0) \frac{dH(\mu)}{d\mu} \right) \right]. \quad (21)$$

The derivative of the angular flux with respect to any quantity  $B$  can then be defined using the chain rule, i.e.,  $\frac{dH}{dB} = \frac{dH}{dc} \frac{dc}{dB}$ , as long as  $\frac{dc}{dB}$  is known:

$$\frac{d\psi(0, -\mu)}{dB} = \frac{\mu_0}{2(\mu + \mu_0)} \frac{dc}{dB} \left[ H(\mu_0)H(\mu) + c \left( \frac{dH(\mu_0)}{d\mu_0} H(\mu) + H(\mu_0) \frac{dH(\mu)}{d\mu} \right) \right]. \quad (22)$$

The value of  $\frac{dc}{dB}$  is given for two quantities  $B$  and two different definitions of the scattering ratio in Table I. The physics is that  $c := \frac{\sigma_s}{\sigma_s + \sigma_a}$ , with  $\sigma_t = \sigma_s + \sigma_a$ .

TABLE I. Values of  $\frac{dc}{dB}$  for  $c := \frac{\sigma_s}{\sigma_s + \sigma_a}$

Definition	Evaluation
$\frac{dc}{d\sigma_a}$	$-\frac{\sigma_s}{\sigma_t^2}$
$\frac{dc}{d\sigma_s}$	$-\frac{\sigma_a}{\sigma_t^2}$

Scalar flux  $\phi$  is solved by numerically integrating over angle using Gauss-Legendre quadrature:

$$\phi(0) \approx \sum_{n=1}^N \psi(0, -\mu_n) w_n. \quad (23)$$

We use the same quadrature order  $N$  for the angular integration as for the  $H$ -function evaluation, though this would not be necessary. Similarly, the derivative of the scalar flux with respect to quantity  $B$  is found by numerically integrating the derivative of the angular flux:

$$\frac{d\phi(0)}{dB} \approx \sum_{n=1}^N \frac{d\psi(0, -\mu_n)}{dB} w_n, \quad (24)$$

which can expand to

$$\frac{d\phi(0)}{dB} \approx \frac{\mu_0}{2} \frac{dc}{dB} \sum_{n=1}^N \frac{w_n}{\mu_n + \mu_0} \left[ H(\mu_0)H(\mu_n) + c \left( \frac{dH(\mu_0)}{d\mu_0} H(\mu_n) + H(\mu_0) \frac{dH(\mu_n)}{d\mu_n} \right) \right], \quad (25)$$

and can be shown to be equal to

$$\frac{d\phi(0)}{dB} \approx \frac{\mu_0 H(\mu_0)}{2} \frac{dc}{dB} \sum_{n=1}^N \frac{w_n H(\mu_n)}{\mu_n + \mu_0} \left[ 1 + \mu_0 \sum_{i=1}^N \frac{a_i H(s_i^{-1})}{1 + s_i\mu_0} + \mu_n \sum_{i=1}^N \frac{a_i H(s_i^{-1})}{1 + s_i\mu_n} \right]. \quad (26)$$

## 1. Combined Sensitivities and Perturbations

Table II compares fluxes and sensitivities at the material boundary for the semi-analytic solution (SA) and the Monte Carlo results (MC). Sensitivities are shown for the scattering cross section ( $\Sigma_s$ ) with finite perturbations in both the scattering and total cross sections ( $\Sigma_t$ ). Based on increasing quadrature orders, the semi-analytic results were converged to about 14 digits at quadrature order of  $N=100$ . All Monte Carlo results were obtained in a single calculation using  $2 \times 10^9$  particle histories. The Monte Carlo statistical uncertainties (MC+-) and error in the Monte Carlo results (MC-SA) are within reasonable statistical agreement.

We do not show results here for the absorption and total cross-section sensitivities but have examined those as well. The absorption cross-section sensitivities are the same magnitude but opposite sign of the scattering cross-section sensitivities. From the definition of the problem we know that the result is the same for any value of the total cross section. Therefore, we expect the sensitivity to the total cross section to be zero (if the scattering and absorption are varied proportionally). The Monte Carlo estimates of sensitivity to the total cross section provide the expected results, with estimates that are in statistical agreement with a value of zero and converging toward zero with increasing histories.

It is known that the correlated-sampling approach can become unstable for large scattering ratios [4]. The stability depends on the choice of the nominal state from which the perturbation is being evaluated. Using the cross section values with the highest scattering ratio ( $c = 0.9333$ ) as the nominal case allowed all perturbations to be evaluated accurately, and these results are shown in Table II. We found that using the mid-point values for the cross sections ( $c = 0.5$ ) caused evaluation of the point with the highest scattering ratio to be difficult to converge (i.e., it produced inaccurate results with misleading statistical uncertainty estimates), and these results are shown in Table III. To further explore the behavior, we performed the same calculations with the nominal case using the lowest scattering ratio ( $c = 0.24$ ), and these results are shown in Table IV. Comparison of the tables shows the increasing errors and statistical uncertainties as the scattering ratio of the nominal case is decreased. We also observed that the statistical uncertainty estimates became less reliable.

## IV. RESULTS AND ANALYSIS

In the results below we report sensitivities,  $S_i$ , in a unitless quantity as relative change in a response,  $R$ , per relative change in a parameter,  $p_i$ :

$$S_i = \frac{p_i}{R} \frac{\partial R}{\partial p_i}. \quad (27)$$

For the full-physics simulations, we calculate sensitivity to material density and eight cross sections. For photons, these include photo-ionization, incoherent scattering, and coherent scattering. For electrons, these include electro-ionization, electronic excitation, bremsstrahlung, large-angle elastic scattering, and small-angle elastic scattering. We divide electron elastic scattering into large and small angles at  $\mu_{cut} = 0.9$  and approximate the small-angle scattering with a single discrete

angle (as described in [9]).

To determine whether sensitivities are being evaluated accurately by the differential-operator method, the central-difference method was used:

$$S_i \approx \frac{p_i}{R(p_i)} \frac{R(p_i + \Delta p) - R(p_i - \Delta p)}{2\Delta p}. \quad (28)$$

The calculations were performed with values of the cross sections perturbed by  $\pm 10\%$  (for the Dolan data) or  $\pm 1\%$  (for the McLaughlin data).

### 1. Photon-Electron Transport Sensitivities

The Dolan validation experiments [16] consisted of bremsstrahlung photon spectra incident on slabs of material and measured the forward and backward emitted electrons. Calculations were performed with  $10^{10}$  particle histories. While energy spectra were also measured, here we compare against only the integral quantities. The number of forward-emitted electrons (per uncollided transmitted photon) measured for a 50 keV spectrum incident on 0.16 cm of tantalum was  $6.3E-3 \pm 9E-4$ , and we calculate  $5.860E-3 \pm 1E-6$ . The number of backward-emitted electrons (per incident photon) measured for 0.16 cm of tantalum was  $5.3E-3 \pm 8E-4$ , and we calculate  $4.5338E-3 \pm 7E-7$ . The uncertainties for calculated values reflect only the Monte Carlo statistical uncertainty.

We also calculated sensitivities to density and interaction cross sections. Results are given in Table V. As might be expected, the electron emission is almost linearly sensitive to the photo-ionization cross section. The next highest sensitivities are electro-ionization, large-angle elastic scattering, electronic excitation, and small-angle elastic scattering. Change in electron emission is positively correlated with changes in the photon cross sections and negatively correlated with changes in the electron cross sections. Reasonable agreement was found between the sensitivities calculated by the differential-operator and central-difference methods. Very small sensitivities were found for photon coherent scattering, photon incoherent scattering, and bremsstrahlung interactions, and the central-difference technique did not achieve acceptable statistical-uncertainty levels to evaluate the accuracy of these sensitivities.

### 2. Electron Transport Sensitivities

The tests of McLaughlin [17] used normally incident, monoenergetic electrons and measured energy deposition as a function of depth through material slabs. We examine the case of 100 keV electrons incident on polystyrene. For polystyrene, we used a composition of 7.7418 weight percent hydrogen, 92.2582 weight percent carbon, and a density of  $1.06 \text{ g/cm}^3$ . The energy deposition profile calculated with ITS is compared with the experimental data in Fig. 1. Sensitivities of the energy deposition to the density and elemental weight fractions are shown as a function of depth in Fig. 2. Sensitivities of the energy deposition to selected interaction cross sections are shown in Fig. 3. Each figure also includes the percent relative statistical uncertainty in the associated quantities. Poor statistical convergence is achieved on most quantities beyond a

TABLE II. Flux and Sensitivity Values from Semi-Analytic (SA) and Monte Carlo (MC) Solutions with the Nominal Monte Carlo Simulation Using  $\Sigma_s = 0.7$  and  $\Sigma_t = 0.75$

$\Sigma_s$	$\Sigma_t$	Boundary Flux, $\phi(0)$				Sensitivity, $\frac{\Sigma_s}{\phi(0)} \frac{d}{d\Sigma_s} \phi(0)$			
		SA	MC	MC+-	MC-SA	SA	MC	MC+-	MC-SA
0.3	0.75	1.1833807	1.1833847	1.7E-5	4.1E-6	0.1249053	0.1249041	1.2E-5	-1.2E-6
0.3	1	1.1268444	1.1268455	1.3E-5	1.1E-6	0.0968566	0.0968580	8.9E-6	1.4E-6
0.3	1.25	1.0970673	1.0970686	1.1E-5	1.3E-6	0.078823	0.078831	7.8E-6	8.0E-6
0.5	0.75	1.404659	1.404675	3.2E-5	1.6E-5	0.180548	0.180565	1.9E-5	1.7E-5
0.5	1	1.2512596	1.2512649	2.3E-5	5.4E-6	0.149771	0.149781	1.6E-5	9.9E-6
0.5	1.25	1.1833807	1.1833846	1.9E-5	3.9E-6	0.124905	0.124915	1.4E-5	9.7E-6
0.7	0.75	1.98659	1.98664	5.8E-5	5.3E-5	0.152348	0.152373	5.0E-5	2.4E-5
0.7	1	1.444746	1.444768	3.6E-5	2.2E-5	0.184332	0.184363	2.4E-5	3.1E-5
0.7	1.25	1.299354	1.299366	2.8E-5	1.2E-5	0.162697	0.162724	2.0E-5	2.6E-5

TABLE III. Flux and Sensitivity Values from Semi-Analytic (SA) and Monte Carlo (MC) Solutions with the Nominal Monte Carlo Simulation Using  $\Sigma_s = 0.5$  and  $\Sigma_t = 1.0$

$\Sigma_s$	$\Sigma_t$	Boundary Flux, $\phi(0)$				Sensitivity, $\frac{\Sigma_s}{\phi(0)} \frac{d}{d\Sigma_s} \phi(0)$			
		SA	MC	MC+-	MC-SA	SA	MC	MC+-	MC-SA
0.3	0.75	1.183381	1.183359	2.4E-5	-2.1E-5	0.124905	0.124894	2.2E-5	-1.1E-5
0.3	1	1.126844	1.126827	1.7E-5	-1.8E-5	0.0968566	0.0968515	1.3E-5	-5.1E-6
0.3	1.25	1.097067	1.097055	1.4E-5	-1.3E-5	0.0788234	0.0788180	1.1E-5	-5.4E-6
0.5	0.75	1.4046586	1.4046647	6.2E-5	6.0E-6	0.180548	0.180526	1.3E-4	-2.2E-5
0.5	1	1.251260	1.251238	3.0E-5	-2.2E-5	0.149771	0.149784	2.5E-5	1.3E-5
0.5	1.25	1.183381	1.183362	2.4E-5	-1.9E-5	0.1249053	0.1249063	1.9E-5	1.0E-6
0.7	0.75	1.9866	1.9645	4.7E-3	-2.2E-2	0.1523	0.1416	6.6E-3	-1.1E-2
0.7	1	1.4447461	1.4447484	6.1E-5	2.2E-6	0.184332	0.184306	8.9E-5	-2.6E-5
0.7	1.25	1.299354	1.299335	3.7E-5	-1.9E-5	0.1626974	0.1627004	3.5E-5	3.0E-6

TABLE IV. Flux and Sensitivity Values from Semi-Analytic (SA) and Monte Carlo (MC) Solutions with the Nominal Monte Carlo Simulation Using  $\Sigma_s = 0.3$  and  $\Sigma_t = 1.25$

$\Sigma_s$	$\Sigma_t$	Boundary Flux, $\phi(0)$				Sensitivity, $\frac{\Sigma_s}{\phi(0)} \frac{d}{d\Sigma_s} \phi(0)$			
		SA	MC	MC+-	MC-SA	SA	MC	MC+-	MC-SA
0.3	0.75	1.18338	1.18353	6.2E-5	1.5E-4	0.12491	0.12501	5.9E-5	1.0E-4
0.3	1	1.12684	1.12692	2.8E-5	7.8E-5	0.096857	0.096913	2.2E-5	5.6E-5
0.3	1.25	1.09707	1.09712	2.0E-5	5.1E-5	0.078823	0.078859	1.7E-5	3.5E-5
0.5	0.75	1.40466	1.40472	6.2E-4	5.7E-5	0.1805	0.1821	1.6E-3	1.5E-3
0.5	1	1.25126	1.25150	7.3E-5	2.4E-4	0.14987	0.15002	1.6E-4	2.5E-4
0.5	1.25	1.18338	1.18349	3.9E-5	1.1E-4	0.124905	0.124971	4.8E-5	6.6E-5
0.7	0.75	1.987	1.905	1.5E-2	-8.1E-2	0.152	0.164	2.3E-2	1.2E-2
0.7	1	1.4447	1.4458	1.1E-3	1.0E-3	0.1843	0.1860	3.2E-3	1.7E-3
0.7	1.25	1.29935	1.29969	1.5E-4	3.4E-4	0.1627	0.1632	5.4E-4	5.3E-4

depth of about 17 mg/cm<sup>2</sup>, where very little energy deposition is calculated. Depths greater than 17 mg/cm<sup>2</sup> are beyond the range of the incident electrons, and energy deposition at those depths depends on bremsstrahlung and fluorescence photon transport.

The results show expected trends, with greater sensitivity to interactions with carbon than with hydrogen and the greatest sensitivity due to the electro-ionization cross section of carbon. In general, increasing one of the cross sections (proportionally across all energies) will result in greater deposition at the

front of the slab and much less deposition near the maximum electron range. Poor statistical convergence is also found for sensitivities at a depth of about 8 mg/cm<sup>2</sup>, where the calculated sensitivities are near zero.

The accuracy of the sensitivity for the carbon electro-ionization is compared to results obtained using the central-difference method in Fig. 4. Agreement is generally within 10% in regions where good statistical convergence was achieved.

TABLE V. Cross Section Sensitivities for Forward and Backward Electron Emission Using Differential Operator (DO) and Central Difference (CD), with Integer Percent Relative Statistical Uncertainty in Parentheses

Cross Section	Backward		Forward	
	DO	CD	DO	CD
Photo-ionization	9.89E-1 (0)	9.88E-1 (0)	9.74E-1 (0)	9.74E-1 (0)
Coherent	6.31E-3 (0)	7.37E-3 (15)	8.47E-3 (0)	5.39E-3 (25)
Incoherent	2.21E-3 (0)	3.26E-3 (33)	1.28E-3 (1)	-8.41E-5 (99)
Electro-ionization	-6.00E-1 (0)	-6.01E-1 (0)	-4.93E-1 (0)	-4.94E-1 (0)
Excitation	-1.36E-1 (1)	-1.35E-1 (1)	-1.10E-1 (2)	-1.09E-1 (1)
Bremsstrahlung	-2.08E-3 (1)	-2.28E-3 (47)	-1.86E-3 (1)	-2.02E-3 (66)
Small Elastic	-4.24E-2 (2)	-4.20E-2 (3)	-7.94E-2 (1)	-8.26E-2 (2)
Large Elastic	-2.25E-1 (0)	-2.24E-1 (0)	-3.15E-1 (0)	-3.24E-1 (0)

## V. CONCLUSIONS

We are investigating the differential-operator and correlated-sampling methods to enable more efficient and more rigorous uncertainty quantification for electron-photon transport. Comparisons with a semi-analytic benchmark have demonstrated the accuracy of the methods in combination. Preliminary evaluations of test problems have demonstrated the differential-operator method with electron and coupled photon-electron transport. We intend to further develop and test these methods within the ITS code. Further evaluation is needed to assess whether the correlated-sampling approach will be valuable for practical electron transport applications or can be useful if applied only to photon cross sections.

A promising approach that we have not yet explored for the calculation of sensitivities in these problems is adjoint-weighted tallies in forward simulations. This approach has been extensively developed for criticality calculations [18]. It has only been demonstrated for fixed-source calculations in limited regimes, using the Iterated Fission Probability method for an adjoint estimator in problems involving multiplying media [19] or in problems involving only uncollided radiation [20].

## VI. ACKNOWLEDGMENTS

Supported by the Laboratory Directed Research and Development program at Sandia National Laboratories, a multi-mission laboratory managed and operated by Sandia Corporation, a wholly owned subsidiary of Lockheed Martin Corporation, for the U.S. Department of Energy's National Nuclear Security Administration under contract DE-AC04-94AL85000.

## REFERENCES

1. M. C. G. HALL, "Cross-Section Adjustment with Monte Carlo Sensitivities: Application to the Winfrith Iron Benchmark," *Nucl. Sci. Eng.*, **81**, 423–431 (1982).
2. B. M. ADAMS ET AL., "Dakota, A Multilevel Parallel Object-Oriented Framework for Design Optimization, Parameter Estimation, Uncertainty Quantification, and Sensitivity Analysis: Version 6.4 User's Manual," Tech. Rep. SAND2014-4633, Sandia National Laboratories (2016).
3. B. M. ADAMS ET AL., "Adjoint-enabled Uncertainty

Quantification for Satellite Shield Designs," in "M&C 2017," Jeju, South Korea (April 2017).

4. H. RIEF, "Generalized Monte Carlo Perturbation Algorithms for Correlated Sampling and a Second-Order Taylor Series Approach," *Ann. Nucl. Energy*, **11**, 9, 455–476 (1984).
5. I. LUX and L. KOBLINGER, *Monte Carlo Particle Transport Methods: Neutron and Photon Calculations*, CRC Press (1991).
6. A. K. HESS ET AL., "Verification of the MCNP Perturbation Correction Feature for Cross-Section Dependent Tallies," Tech. Rep. LA-13520, Los Alamos National Laboratory (1998).
7. B. C. FRANKE and A. K. PRINJA, "Monte Carlo Solution for Uncertainty Propagation in Particle Transport with a Stochastic Galerkin Method," in "M&C 2013," Sun Valley, ID (May 2013).
8. A. J. OLSON, B. C. FRANKE, and A. K. PRINJA, "Scaling of Intrusive Stochastic Collocation and Stochastic Galerkin Methods for Uncertainty Quantification in Monte Carlo Particle Transport," in "M&C 2015," Nashville, TN (April 2015).
9. D. M. FLETCHER and B. C. FRANKE, "Generalised Boltzmann Fokker-Planck Elastic Scattering using the Evaluated Electron Data Library," in "M&C 2017," Jeju, Korea (April 2017).
10. B. C. FRANKE ET AL., "ITS Version 6: The Integrated TIGER Series of Coupled Electron/Photon Monte Carlo Transport Codes," Tech. Rep. SAND2008-3331, Sandia National Laboratories (2013).
11. S. PERKINS and D. CULLEN, "ENDL type formats for Evaluated Atomic Data Library, EADL, for the Evaluated Electron Data Library, EEDL, and for the Evaluated Photon Data Library, EPDL," Tech. Rep. UCRL-ID-117796, Lawrence Livermore National Laboratory (1994).
12. H. RIEF, "A Synopsis of Monte Carlo Perturbation Algorithms," *J. Comp. Phys.*, **111**, 33–48 (1994).
13. B. D. GANAPOL, *Analytical Benchmarks for Nuclear Engineering Applications*, Organisation for Economic Co-operation and Development (2008).
14. T. VIHK, "An Efficient Method to Calculate Ambarzumian-Chandrasekhar's and Hopf's Functions," *Astrophys. Space Sci.*, **127**, 2, 285–307 (1986).

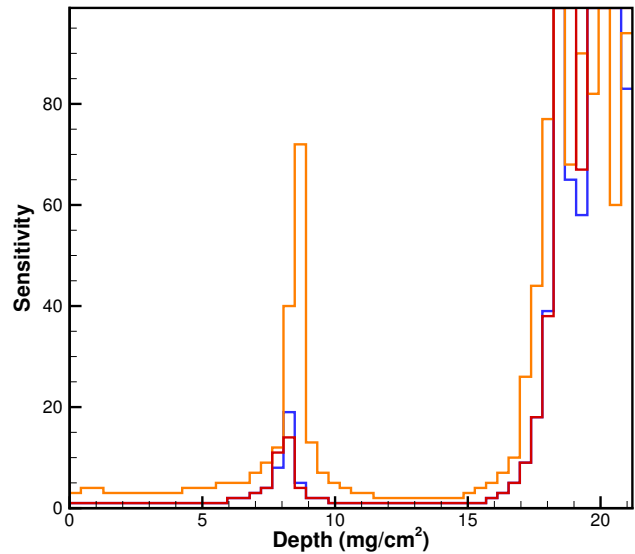
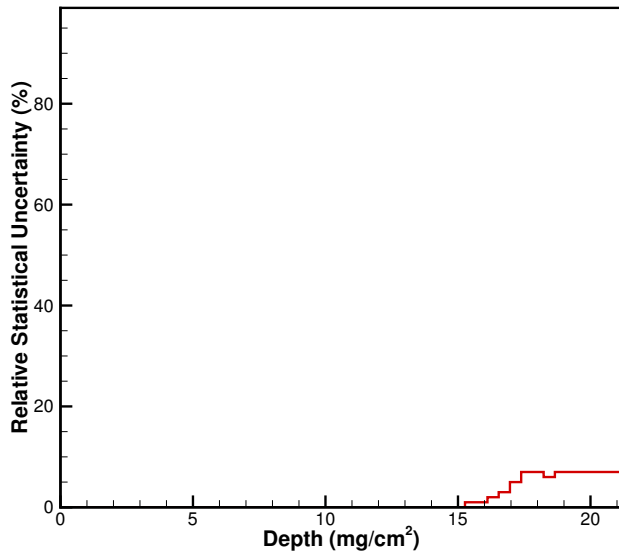
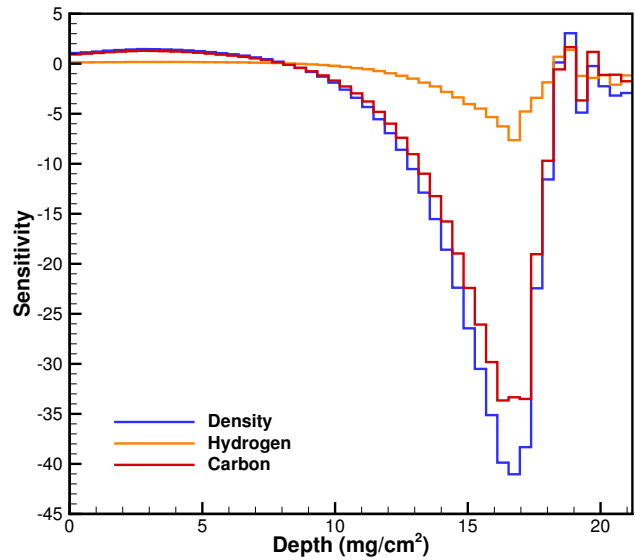
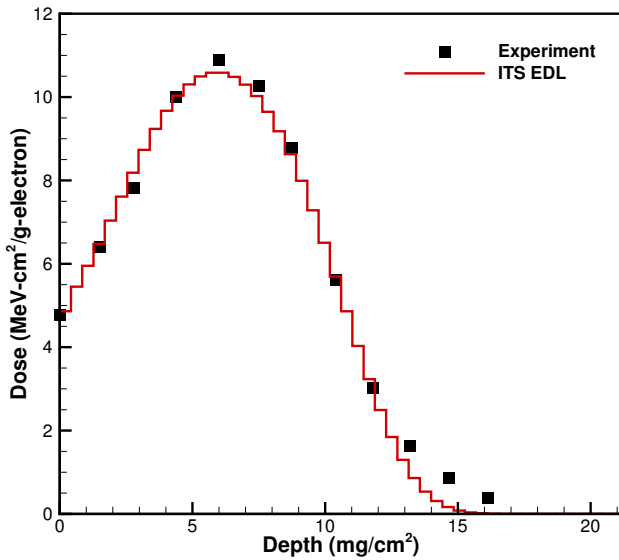


Fig. 1. (a) ITS energy deposition compared to experimental data and (b) corresponding relative statistical uncertainty.

Fig. 2. (a) Sensitivity of energy deposition to the density and relative weight fractions of hydrogen and carbon and (b) corresponding relative statistical uncertainty.

15. T. VIHK, "Derivatives of the  $H$ -Function," *Astrophys. Space Sci.*, **204**, 2, 213–231 (1993).
16. K. W. DOLAN, "X-ray-Induced Electron Emission from Metals," *J. Appl. Phys.*, **46**, 6, 2456–2463 (1975).
17. W. L. MCLAUGHLIN and E. K. HUSSMAN, "The Measurement of Electron and Gamma-Ray Dose Distributions in Various Media," in "Large Radiation Sources for Industrial Processes," IAEA-SM-123/43.
18. B. C. KIEDROWSKI and F. B. BROWN, "Adjoint-Based  $k$ -Eigenvalue Sensitivity Coefficients to Nuclear Data Using Continuous-Energy Monte Carlo," *Nucl. Sci. Eng.*, **174**, 227–244 (2012).
19. B. C. KIEDROWSKI and A. SOOD, "Prototype Fixed-Source Sensitivity Capability in MCNP6 Applied to Sub-

- critical Thor Core Measurements," *Trans. Am. Nucl. Soc.*, **109** (2013).
20. J. A. FAVORITE, K. C. BLEDSOE, and D. I. KETCHESON, "Surface and Volume Integrals of Uncollided Adjoint Fluxes and Forward-Adjoint Flux Products," *Nucl. Sci. Eng.*, **163**, 73–84 (2009).

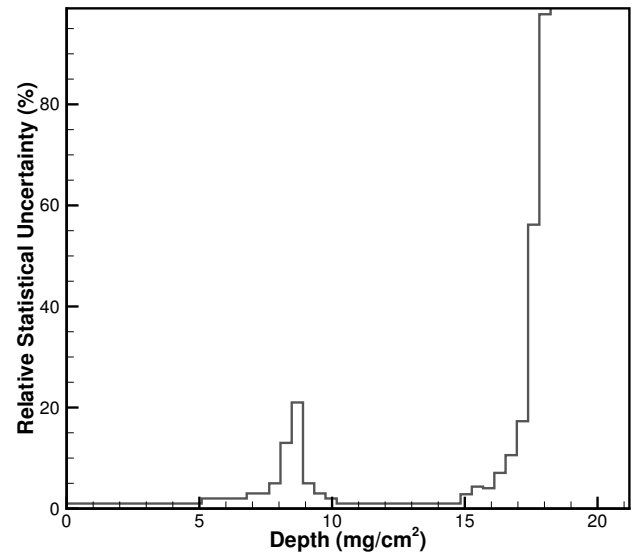
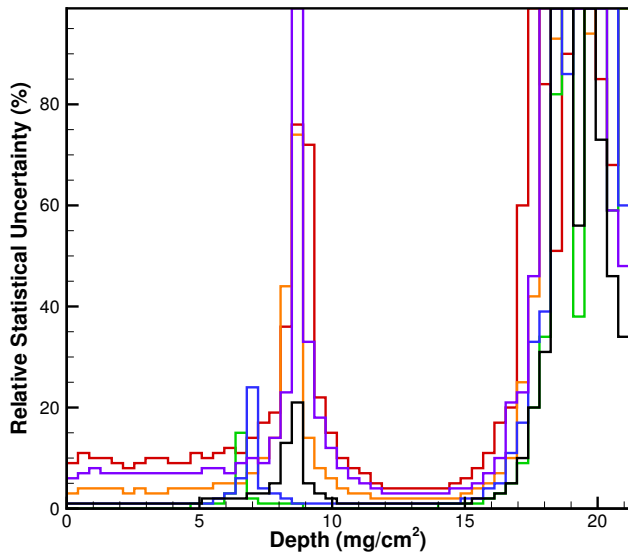
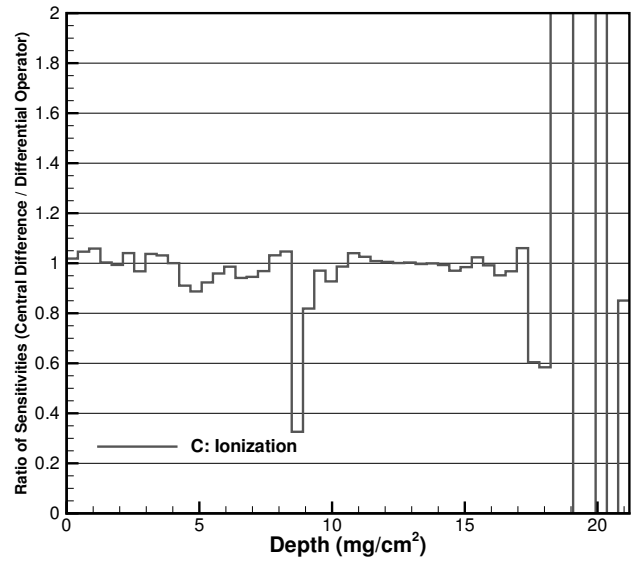
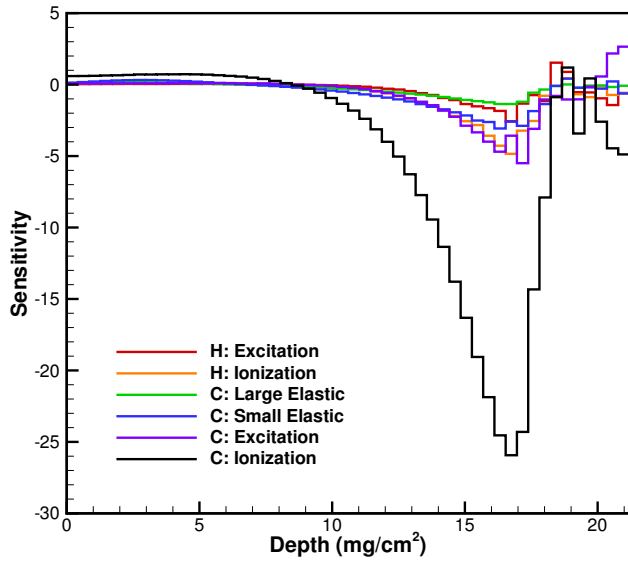


Fig. 3. (a) Sensitivity of energy deposition to selected electron cross sections of hydrogen and carbon and (b) corresponding relative statistical uncertainty.

Fig. 4. (a) Ratio of sensitivities calculated by central difference and differential operator methods for electron ionization of carbon and (b) corresponding relative statistical uncertainty.